Coral Reefs (2012) 31:741–752
DOI 10.1007/s00338-012-0890-3

REPORT

Pulsed ^{86}Sr-labeling and NanoSIMS imaging to study coral biomineralization at ultra-structural length scales

C. Brahmi · I. Domart-Coulon · L. Rougée · D. G. Pyle · J. Stolarski · J. J. Mahoney · R. H. Richmond · G. K. Ostrander · A. Meibom

Received: 24 August 2011 / Accepted: 11 February 2012 / Published online: 1 March 2012

Abstract A method to label marine biocarbonates is developed based on a concentration enrichment of a minor stable isotope of a trace element that is a natural component of seawater, resulting in the formation of biocarbonate with corresponding isotopic enrichments. This biocarbonate is subsequently imaged with a NanoSIMS ion microprobe to visualize the locations of the isotopic marker on sub-micrometric length scales, permitting resolution of all ultra-structural details. In this study, a scleractinian coral, *Pocillopora damicornis*, was labeled 3 times with ^{86}Sr-enhanced seawater for a period of 48 h with 5 days under normal seawater conditions separating each labeling event. Two non-specific cellular stress biomarkers, glutathione-S-transferase activity and porphyrin concentration plus carbonic anhydrase, an enzymatic marker involved in the physiology of carbonate biomineralization, as well as unchanged levels of zooxanthellae photosynthesis efficiency indicate that coral physiological processes are not affected by the ^{86}Sr-enhancement. NanoSIMS images of the ^{86}Sr/^{44}Ca ratio in skeleton formed during the experiment allow for a determination of the average extension rate of the two major ultra-structural components of the coral skeleton: Rapid Accretion Deposits are found to form on average about 4.5 times faster than Thickening Deposits. The method opens up new horizons in the study of biocarbonate formation because it holds the potential to observe growth of calcareous structures such as skeletons, shells, tests, spines formed by a wide range of organisms under essentially unperturbed physiological conditions.

Keywords Biomineralization · Scleractinia · Skeleton · ^{86}Sr-labeling · Growth dynamics · Ecotoxicology

Communicated by Biology Editor Dr. Mark Warner

Electronic supplementary material The online version of this article (doi:10.1007/s00338-012-0890-3) contains supplementary material, which is available to authorized users.

C. Brahmi (✉) · A. Meibom
Laboratoire de Minéralogie et Cosmochimie du Muséum UMR7202, Muséum National d'Histoire Naturelle, 61 rue Buffon, CP 52, 75005 Paris, France
e-mail: cbrahmi@mnhn.fr

C. Brahmi · I. Domart-Coulon
Laboratoire de Biologie des Organismes et Ecosystèmes Aquatiques UMR7208, Muséum National d'Histoire Naturelle, 43 rue Cuvier, 75005 Paris, France

L. Rougée · R. H. Richmond
Pacific Biosciences Research Center, University of Hawaii at Mano'a—Kewalo Marine Laboratory, 41 Ahui Street, Honolulu, HI 96813, USA

D. G. Pyle · J. J. Mahoney
Department of Geology and Geophysics, University of Hawaii at Mano'a, 1680 East West Road, Honolulu, HI 96822, USA

J. Stolarski
Institute of Paleobiology, Polish Academy of Sciences, ul. Twarda 51/55, 00-818 Warszawa, Poland

G. K. Ostrander
Pacific Biosciences Research Center, University of Hawaii at Mano'a, 2500 Campus Road, Honolulu, HI 96822, USA

A. Meibom (✉)
Laboratory for Biological Geochemistry, Ecole Polytechnique Fédérale de Lausanne, ENAC IIE LGB, 1015 Lausanne, Switzerland
e-mail: anders.meibom@epfl.ch

Introduction

Marine biocarbonates such as coral skeletons, foraminifera tests, mollusks and brachiopods shells have been a subject of intense scientific interest since it was realized that their chemical (e.g., Mg/Ca, Sr/Ca, Ba/Ca) and isotopic compositions (e.g., δ^{11}B, δ^{13}C, δ^{18}O) might provide proxies for marine paleo-environmental changes on both short and long timescales (e.g., Epstein et al. 1953; Smith et al. 1979; Zachos et al. 2001). However, almost without exception, these proxies are affected by biological (so-called vital) effects, which influence or control the composition of the biocarbonate independent of environmental variations, and decrease the precision with which the chemical or isotopic composition record environmental change (Adkins et al. 2003; Rollion-Bard et al. 2003; Sinclair 2005; Blamart et al. 2007; Nothdurft and Webb 2007; Meibom et al. 2008; Allison et al. 2010; Brahmi et al. 2010).

The processes by which the microstructures and composition of biocarbonates are controlled are still poorly understood (Stolarski 2003; Gladfelter 2007). One obstacle has been the lack of a method to study the growth dynamics on the sub-micrometer length scales on which individual structural components form. Labeling techniques with the visible stain alizarin red or the fluorescent marker calcein have been applied to mark the mineralization front in carbonate-producing organisms. Both chemicals form an irreversible complex with calcium carbonate during precipitation and have been widely used to calibrate calcareous skeletal growth on timescales ranging from days/weeks to months/years (Barnes 1972; Guzman and Cortes 1989; Swart et al. 2002; Bernhard et al. 2004; Thébault et al. 2006; Brahmi et al. 2010). Dodge et al. (1984) reported a negative effect of alizarin staining (10 mg l^{-1} for 24 h) on the calcification rate of the zooxanthellate scleractinian coral *Diploria strigosa*, for a period of up to 6 days following the exposure. A qualitatively similar observation was made on *Pocillopora damicornis* (Allison et al. 2011). Calcein is usually considered non-lethal at low doses (50 μM l^{-1}–10 mg l^{-1}) for adult corals (Brahmi et al. 2010) or foraminifera (Bernhard et al. 2004), but could induce behavioral stress or death, especially of juveniles and larvae of fishes (Bumguardner and King 1996) and bivalves (Thébault et al. 2006). One recent study found that calcein labeling does not alter trace element incorporation (Mg and Sr) in the skeletal calcite of foraminifera tests (Dissard et al. 2009). However, the calcein fluorescent label is diffusely distributed and its emission intensity fades with time, which complicates its detection and superposition onto ultra-structural observations.

Radioactive isotopes, in particular ^{14}C, ^{45}Ca, ^{85}Sr and ^{90}Sr, have been used since the 1970s to quantify scleractinian coral calcification rates based on bulk analysis of entire corallites or colony fragments (Goreau 1959; Clausen and Roth 1975) and to investigate uptake and pathways of Ca (Tambutté et al. 1996; Marshall and Clode 2002) and Sr (Ip and Krishnanevi 1991; Ferrier-Pagès et al. 2002). Marshall and Wright (1998) used autoradiography of sections (0.5 mm thick) of labeled *Galaxea fascicularis* polyps in an attempt to localize specific sites of uptake into individual corallites with a spatial resolution in the sub-millimeter range, which is insufficient to resolve sub-micrometer ultra-structural components inside the skeleton.

Here, we describe an experimental method to precisely label biocarbonates with high spatial and temporal resolution. In this study, the method is based on the incorporation of the stable isotope ^{86}Sr, a natural component of seawater, into the aragonitic skeleton of a living scleractinian coral *P. damicornis* (Linnaeus 1758) with subsequent imaging of the enhanced ^{86}Sr abundances in the skeleton using the high spatial resolution of NanoSIMS ion microprobe. The feasibility of this method was recently documented in a pilot study of the scleractinian coral *Porites porites*. (Houlbrèque et al. 2009). In the present study, we have quantified the ^{86}Sr-enrichment factor of the labeled seawater with thermal ionization mass spectrometry (TIMS) and tested whether coral physiology was affected by an increase in Sr-concentration using complementary bio-indicators of ecotoxicological stress. NanoSIMS observations of the skeletal structures formed during ^{86}Sr-labeling allow growth dynamics to be compared between different ultra-structural components at different levels in the corallite. The observations obtained from this study provide an excellent basis for further developing and refining the method.

Materials and methods

Biological material

The scleractinian coral *P. damicornis*, a tropical (Indo–Pacific) colonial zooxanthellate reef-building species, was collected off the south shore of Coconut Island (Kanehoe Bay, Hawaii) under Special Activities Permit 2009-42 (Department of Land and Natural Resources under the Division of Aquatic Resources). Thirty nubbins (branch tips ~4 cm height, ~3 cm wide) were prepared from the same parent colony (=same genotype) and acclimatized on outdoor water tables with running seawater at Kewalo Marine Laboratory (University of Hawaii, USA) for 8 weeks. Experiments were conducted under ambient light, 25 ± 1 (SD)°C temperature and 36 ± 1 (SD)‰ salinity conditions during May 2010 on healthy nubbins completely covered with tissue.

Strontium dose–response experiment

Strontium is a trace element present in seawater in concentrations of about 8 ppm ($\sim 9 \times 10^{-5}$ mol l^{-1}) (Chow and Thompson 1955; de Villiers 1999) and is known to substitute for Ca in the aragonite structure (Finch and Allison 2002).

To detect an effect of increased Sr-concentration in seawater on the coral physiology, a dose–response experiment was carried out with three increasing doses of isotopically normal Sr. Four replicate nubbins were exposed to each of the enhanced Sr-concentrations (~ 16, ~ 97 and ~ 186 ppm, respectively) for a time interval (48 h) and experimental conditions similar to those used in the subsequent ^{86}Sr labeling experiment. Four other nubbins served as controls and were exposed to normal seawater.

An additional experiment was performed to monitor long-term effects of the highest Sr-dose. Three nubbins were exposed for 2 days to ~ 186 ppm Sr with three control nubbins exposed to normal seawater. Subsequently, all six nubbins were placed back into the main holding tank and monitored every day for 15 days for potential changes in tissue coverage, color, and tentacles extension.

Seawater was enriched in Sr by dissolving isotopically normal $SrCO_3$ (Sigma-Aldrich 99.995% purity) in 1 liter of seawater as follows: (1) 15 mg, (2) 150 mg and (3) 300 mg of $SrCO_3$ were covered with 1 ml de-ionized water to which was added (1) 2 ml of 0.1 N HCl; (2) 2 ml of 1 N HCl and 0.55 ml of 2 N HCl; (3) 1 ml of 1 N HCl and 1.6 ml of 2 N HCl, respectively. These three slightly acidic Sr solutions were ultrasonicated for 10–30 min and subsequently diluted to 1 l with normal, filtered (0.2 μm) seawater yielding isotopically normal seawater with Sr-concentrations of ~ 16, ~ 97 and ~ 186 ppm, respectively, equivalent to enrichment factors of roughly 2, 12 and 23, compared with normal seawater (e.g., Kewalo Marine Laboratory water [Sr] $\approx$ 7.6 ppm).

Average pH values measured at 21°C in triplicate with a calibrated electrode (equilibrated to seawater) were: 8.11 ± 0.01 (SD), 8.04 ± 0.01 (SD) and 8.05 ± 0.01 (SD) for the 16, 97 and 186 ppm Sr solutions, respectively, and 8.13 ± 0.01 (SD) for seawater. These values are within natural pH variations of seawater measured in the outdoor aquaria at the Kewalo Marine Laboratory (pH = 8.00–8.14 for T = 23.1–25.5°C) and in the open reef off Coconut Island, Kaneohe Bay (pH = 7.85–8.3 for T = 21.8–26.8°C), and such variations are unlikely to provoke measurable stress on the coral organism (Krief et al. 2010).

Each individual nubbin was incubated for 2 days in a beaker containing 250 ml of Sr-enhanced seawater solution (or control normal seawater) lightly covered with plastic film to limit evaporation and with air bubbling for aeration and water circulation. After 24 h of incubation in the water table (25 ± 1 (SD)°C), 50 ml of the solution was renewed (20% of the volume). After 48 h of exposure, nubbins were individually frozen in liquid nitrogen and then stored at −80°C.

Experimental protocol of ^{86}Sr-labeling

The ^{86}Sr-labeling experiment was conducted over 16 days on four nubbins, with four control nubbins handled in the same way, but exposed to normal seawater. ^{86}Sr-enriched seawater solution was prepared by dissolving ~ 15 mg of ^{86}Sr-carbonate powder ($^{86}SrCO_3$, ^{86}Sr abundance of 97%, Oak Ridge National Laboratory, Tennessee, USA) in 1 l filtered (0.2 μm) seawater as described above. The pH of ^{86}Sr-labeled seawater averaged 8.11 ± 0.01 (SD) ($n = 3$).

For 48 h, each individual nubbin was incubated in 250 ml of ^{86}Sr-enriched seawater ($^{86}Sr/^{88}Sr \sim 1.4$) at 25 ± 1°C under natural light conditions. Air bubbling with a glass Pasteur pipette continuously supplied oxygen to the solution. After 24 h of labeling, 50 ml of the ^{86}Sr-enriched seawater was renewed (20% of the volume in each beaker). At the end of the 48 h period of labeling, all nubbins were transferred back into the main tank with normal, running seawater and grown for 5 days. Then, a second 48-h labeling event was conducted in ^{86}Sr-enriched seawater, after which the microcolonies were transferred back into the tank with normal running seawater and grown for another 5 days. A third and final 48-h labeling event in ^{86}Sr-enriched seawater was carried out after which the experiment was terminated by freezing each nubbin, that is, controls and ^{86}Sr-labeled replicates, in liquid nitrogen to stop all enzymatic reactions in preparation for toxicological assays and skeleton analyses.

Measurements of $^{86}Sr/^{88}Sr$ ratio and total Sr-concentration in seawater solutions

Strontium has four stable isotopes with the following natural isotopic abundances: ^{84}Sr (0.56%), ^{86}Sr (9.86%), ^{87}Sr (7.0%) and ^{88}Sr (82.58%). The ^{86}Sr isotope is therefore only present in seawater at a concentration of about 0.8 ppm. Analyses of strontium concentration and $^{86}Sr/^{88}Sr$ ratio for all solutions used during the experiments were performed on a VG Sector multi-collector TIMS instrument in the Isotopes Laboratory of the Geology and Geophysics Department at the University of Hawaii (USA) following established procedures (de Villiers 1999).

The $^{86}Sr/^{88}Sr$ ratio was measured for all ^{86}Sr-enriched seawater solutions used in the labeling experiment and normal seawater. The Sr-concentrations of the solutions prepared with 15, 150 and 300 mg l^{-1} of normal $SrCO_3$

were determined by isotope dilution and compared to the calculated Sr-concentrations.

Markers of potential stress to the coral organism during experiments

Toxicological assays were performed at the end of the last labeling event in order to test potential cellular stress in response to Sr-enhancements. One oxidative stress and one metabolic stress biomarker were used to indicate a potential shift from cellular homeostasis: Glutathione-S-transferase activity (GST) and porphyrin concentrations were determined for all nubbins (and their controls) in the ^{86}Sr-labeling experiment and for all nubbins (and their controls) in the Sr-dose experiments. Porphyrin concentration was also measured for one unhandled control nubbin that had remained in the large aquarium with normal seawater.

Coral whole cell lysates (WCL) and subcellular (S9) fractions were prepared from coral tissue removed by water-pik and spun at 4°C at 10,000×*g* for 10 min using a Sorvall RC-5B centrifuge, following Downs et al. (2006). Pellets of tissue and cells were homogenized on ice for 1 min in filtered seawater containing 1 mM PMSF (Phenyl Methyl Sulfonyl Fluoride) and centrifuged at 2,000×*g* and 4°C for 5 min. The zooxanthellae pellet was discarded, and supernatant spun again at 2,000×*g* for 3 min. Half of the final supernatant, containing only coral tissue or whole cell lysate (WCL), was stored at −80°C. The other half was homogenized for 2 min, centrifuged at 10,000×*g* and 4°C for 20 min, yielding a supernatant containing the S9 subcellular fraction of coral, which was stored at −80°C. Total protein concentrations of the extracts were quantified colorimetrically using the Bicinchoninic acid protein assay (BCA, Interchim).

Glutathione-S-transferase (GST) activity was determined using the microplate spectrophotometric method from Habig et al. (1974). Coral protein (10 µg of S9 fraction) was pre-incubated (3 min at 37°C) in optically clear microplates with 0.5 mM 1-chloro- 2,4 dinitrobenzene. L-glutathione 1 mM was added, and changes in absorbance per minute were monitored continuously at 340 nm. Total activity was calculated using Beer's Law with $\varepsilon = 9.6\ \mathrm{mM}^{-1}\ \mathrm{cm}^{-1}$. GST enzyme activity was expressed in nmol min^{-1} mg^{-1} protein.

The porphyrin concentration in the coral S9 subcellular fraction was determined following the method of Downs et al. (2006). Briefly, 100 µg of total soluble protein was diluted to 300 µl in Tris–HCl (pH 7.8) containing 5 mM EDTA. Three 100 µl aliquots were distributed into a black fluorescent 96-well microplate. Then, 100 µl of 3 N HCl was added to each well, and the samples were incubated in the dark for 30 min at room temperature. Fluorescence was detected using a Gemini XS fluorescent/luminescent microplate reader (Molecular Devices, Sunnyvale, CA) with an excitation filter at 405 nm and an emission filter at 610 nm. Results were expressed in nmol mg^{-1} of protein using an Uroporphyrin standard curve (Uroporphyrin Fluorescence standards, Frontier Scientific, UFS-1) from 0 to 1,000 nmol.

The carbonic anhydrase (CA) enzyme is involved in numerous physiological reactions including coral biomineralization processes (Goreau 1959; Tambutté et al. 2007a; Moya et al. 2008) and has been used as one marker of stress to coral calcification (Bielmeyer et al. 2010). Total CA activity was assayed for each of the replicate and control nubbins in the ^{86}Sr-labeling experiment using the ΔpH method (Vitale et al. 1999). For each measurement, 7.5 ml of reaction medium (225 mM mannitol, 75 mM sucrose and 10 mM Tris–phosphate pH 7.4) was added to 400 µL of coral tissue extract (300 µg total protein). The decrease in pH was recorded every 10 s for 100 s. The slope of the linear regression of pH versus time, which determines the catalyzed reaction rate (b_c), was determined. The non-catalyzed reaction rate (b_{nc}) was estimated from the pH drop of the control, without tissue-skeleton extract. The carbonic anhydrase activity was calculated for four replicates for each nubbin as $(b_c/b_{nc}-1)$/mg protein and was also measured in the presence of 100 µM acetazolamide (a specific inhibitor of CA) for two replicates for each nubbin.

Potential effect of the ^{86}Sr-labeling protocol on the photophysiology of the symbiotic dinoflagellates (zooxanthellae) was monitored using underwater Pulse Amplitude Modulation (PAM) fluorometry (Walz, Germany) comparing in situ fluorescence yield of photosystem II in zooxanthellae between controls ($n = 4$) and ^{86}Sr-labeled nubbins ($n = 4$) during the second ^{86}Sr-labeling event, after 24 h of exposure. The fluorescence at the steady state (F) and the maximal fluorescence in the light (Fm') were measured, and the apparent quantum yield of photosynthesis ($\Delta F/Fm'$) was calculated, reflecting the efficiency of photosystem II in the light acclimated state (Hoogenboom et al. 2006). For each nubbin, five measurements were collected on the tips of apical branches.

Statistical analyses were performed with the free software "R" (version 2.12.1, http://www.r-project.org). Normality of the data was tested using Shapiro–Wilk test. If the data were normally distributed, a comparison between two treatments was performed via a Student's t test, if not, a Wilcoxon test was used. To compare more than two treatments, a parametric analysis of variance (ANOVA) was performed if the data were normally distributed and with equal variances; otherwise, a nonparametric ANOVA was used. Differences were considered statistically significant for P value <0.05.

NanoSIMS imaging of $^{86}Sr/^{44}Ca$ in the skeleton

Tissue covering the ^{86}Sr-labeled skeleton was removed by blasting with normal, filtered seawater. Analyses of rinsed and dried skeleton were carried out with the Cameca NanoSIMS (Lechene et al. 2006) ion microprobe on polished and gold-coated skeletal surfaces embedded in Körapox® epoxy and cut parallel to the growth axis. Briefly, a primary beam of O^-(40–50 pA) delivered to the sample surface produced secondary ions of $^{86}Sr^+$ and $^{44}Ca^+$ that were transmitted to the mass spectrometer and detected simultaneously in electron multipliers at a mass-resolving power of ~5,000. At this mass-resolving power, any potentially problematic mass interferences are resolved. Images were obtained by rastering across a pre-sputtered surface (to remove the gold coating and establish sputtering equilibrium) with a lateral resolution of the primary beam of about 0.5 μm and comparable pixel size (images of 128 × 128 pixels on a 40 × 40 μm^2 surface area). Count rates for $^{44}Ca^+$ and $^{86}Sr^+$ were typically 15–20 × 10^3 cps and 1,000–1,500 cps, respectively, in unlabeled skeleton. Images of the $^{86}Sr/^{44}Ca$ ratio were obtained by rationing 5 sequential, drift-corrected images of each isotope.

Ultra-structural observations of ^{86}Sr-labeled skeleton

After NanoSIMS analyses, the gold coating was removed and sample surfaces etched for 2 min with a 0.1% formic acid solution following Stolarski (2003). Samples were sputter-coated with conductive platinum film and observed with a Philips XL 20 scanning electron microscope (SEM) at the Polish Academy of Sciences, Warsaw.

Results

Total Sr and ^{86}Sr isotopic enrichment in labeled seawater

Strontium concentration measured for all solutions used during the experiments was in agreement with the calculated Sr-concentrations, indicating that all $SrCO_3$ was dissolved during preparation of the labeled seawater. The three solutions prepared with 15 mg l^{-1} of $^{86}SrCO_3$ yielded $^{86}Sr/^{88}Sr$ values of 1.4151 ± 0.0003 (2σ), 1.3758 ± 0.0006 (2σ) and 1.4096 ± 0.0010 (2σ), respectively, in agreement with the $^{86}Sr/^{88}Sr$ ratio estimated for these solutions and representing an average increase in the $^{86}Sr/^{88}Sr$ ratio by a factor of about 11.6 over that in natural seawater.

Unchanged photophysiology of zooxanthellae symbionts due to the ^{86}Sr-labeling

In situ photosynthesis yield of dinoflagellate symbionts measured with PAM (Pulse Amplitude Modulation) fluorometry in 5 apical branches of each 4 replicate nubbins during the second ^{86}Sr-labeling event indicated a mean of 0.55 ± 0.03 (SD, $n = 20$) for control nubbins versus a mean of 0.54 ± 0.02 (SD, $n = 20$) for ^{86}Sr-labeled nubbins, without any statistically significant difference (t test, $P > 0.05$) (ESM Table 1). Moreover, during all experiments, all nubbins exposed to Sr-labeled seawater and all controls (with one exception) remained brown, with full tissue coverage, polyp tentacles fully extended, and no visual signs of changes in zooxanthellae density.

Absence of cellular oxidative stress due to exposure to strontium

Glutathione-S-transferase (GST) activity data and porphyrin concentrations are presented in Fig. 1 for all nubbins in the total Sr-dose experiments (normal isotopic abundance) and in the ^{86}Sr-labeling experiment (values are listed in Electronic Supplemental Material, ESM Table 1). For the ^{86}Sr-labeling experiment, the GST activity of both controls and ^{86}Sr-labeled nubbins was measured at the end of the last ^{86}Sr-labeling event. No significant differences between controls and nubbins in the Sr-dose and ^{86}Sr-labeling experiments ($P > 0.05$) were detected by either a t test or an analysis of variance (ANOVA). Moreover, no significant difference was detected between GST activities of nubbins exposed to 15 mg l^{-1} of $^{86}SrCO_3$ versus 15 mg l^{-1} of isotopically normal $SrCO_3$ (t test, $P > 0.05$). Levels of GST activity remained unchanged during all of the experiments and fall within the range of GST background levels measured in non-stressed *P. damicornis* nubbins maintained in open seawater systems (data not shown).

Porphyrin concentrations of nubbins exposed to enhanced Sr-concentrations (15, 150 and 300 mg l^{-1}, respectively) were not significantly different from controls exposed to normal seawater (ANOVA test) (Fig. 1). Similarly, no difference was found (t test) for controls versus ^{86}Sr-labeled nubbins ($P > 0.05$). No significant difference was observed between nubbins exposed to 15 mg l^{-1} of isotopically normal $SrCO_3$ and 15 mg l^{-1} of $^{86}SrCO_3$ (t test, $P > 0.05$). The porphyrin concentration of a nubbin prepared from the same parent colony, unhandled and permanently maintained in the running seawater aquarium, was within the range of values measured for all nubbins (and controls) in the Sr-dose response and the ^{86}Sr-labeling experiments. Moreover, during all experiments, some control and test nubbins released a few larvae, as expected for this period in the lunar cycle.

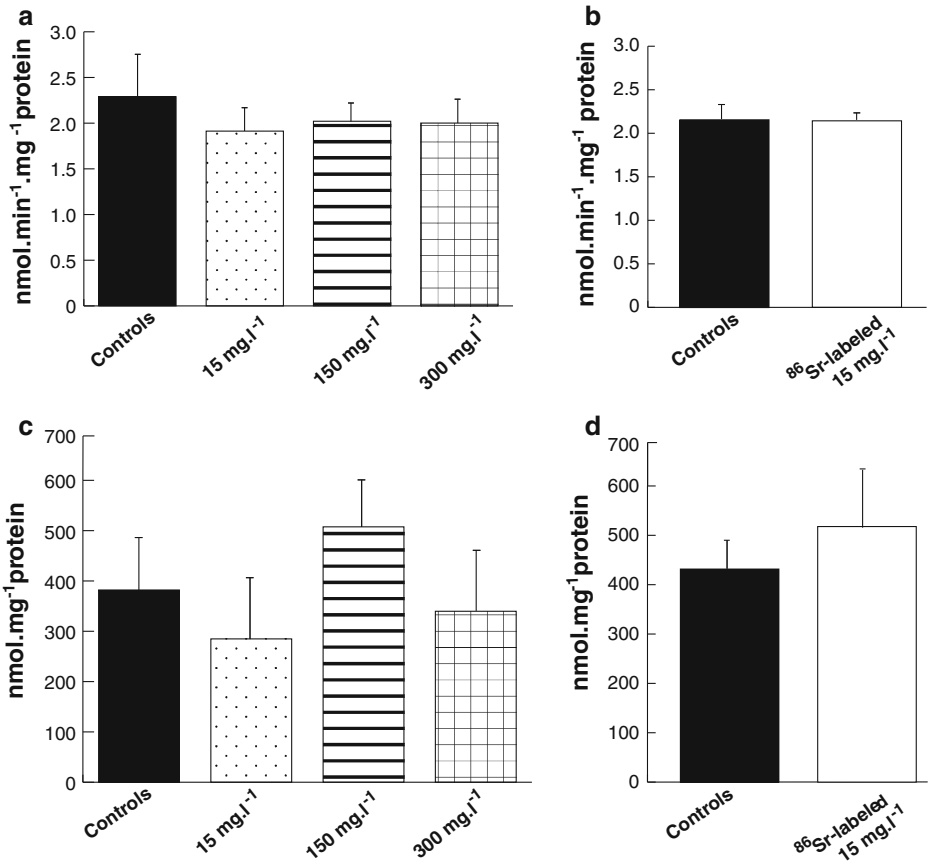

Fig. 1 Cellular stress biomarkers GST activity (**a**, **b**) and porphyrin concentrations (**c**, **d**) in nubbins ($n = 4$) exposed to increasing doses of total Sr (**a**, **c**) and enhanced ^{86}Sr (**b**, **d**), plus their controls. Data represent the mean ± SD. Differences are not significant ($P > 0.05$)

Unchanged levels of carbonic anhydrase activity due to exposure to strontium

Carbonic anhydrase activity was measured to detect a potential effect of increased total Sr-concentration and ^{86}Sr isotope enrichment on enzyme activities involved in the biomineralization process. Results of CA activity assays (4 replicate measurements per nubbin) are presented in Fig. 2

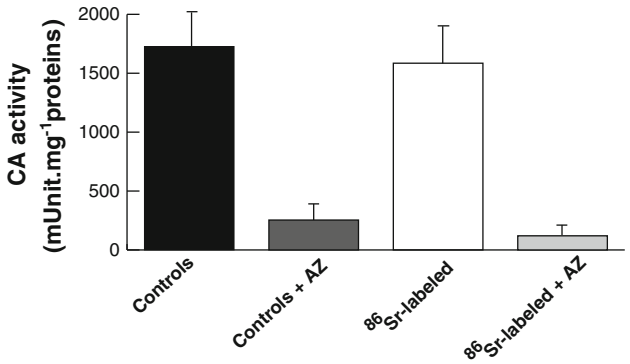

Fig. 2 Carbonic anhydrase activity in control and ^{86}Sr-labeled corals. Specificity of the pH decrease method was confirmed by inhibition by acetazolamide (AZ, 100 μM). Data represent the mean (±SD) of CA activity of controls ($n = 4$) and ^{86}Sr-labeled ($n = 4$) coral nubbins in milliUnits per mg of total proteins. No significant difference between ^{86}Sr-labeled and control nubbins values was detected ($P > 0.05$)

for ^{86}Sr-labeled nubbins ($n = 4$) and for their unlabeled controls ($n = 4$) (values are listed in ESM Material Table 1). Addition of acetazolamide (AZ, 100 μM) resulted in inhibition of CA activity by 85% for controls and by 92% for ^{86}Sr-labeled nubbins, respectively, confirming the specificity of the pH decrease method used. A CA activity of 1727 ± 324 (SD) mU mg^{-1} proteins ($n = 16$) was measured for controls and 1585 ± 350 (SD) mU mg^{-1} proteins ($n = 16$) for ^{86}Sr-labeled nubbins, without statistically significant difference between the two populations ($P > 0.05$).

Distribution of ^{86}Sr in the skeleton of *Pocillopora damicornis*

Images of the $^{86}Sr/^{44}Ca$ distribution in the skeleton of four different ^{86}Sr-labeled nubbins were obtained with the NanoSIMS in longitudinal sections, that is, skeletal surfaces cut parallel to the growth axis. Incorporation of ^{86}Sr was compared between skeletal structures localized at different levels in the colony, including two tips of walls of apical corallites (i.e., at the very top of colony branch) (Figs. $3a_1$, b_1, 4a, 5a) and a spine protruding from the coenosteum surface (i.e., between corallites), 4 mm below the growing tip (Figs. $3b_2$, 5e).

A line profile of the skeletal $^{86}Sr/^{44}Ca$ ratio through the three ^{86}Sr-labeling events shows an enrichment factor of

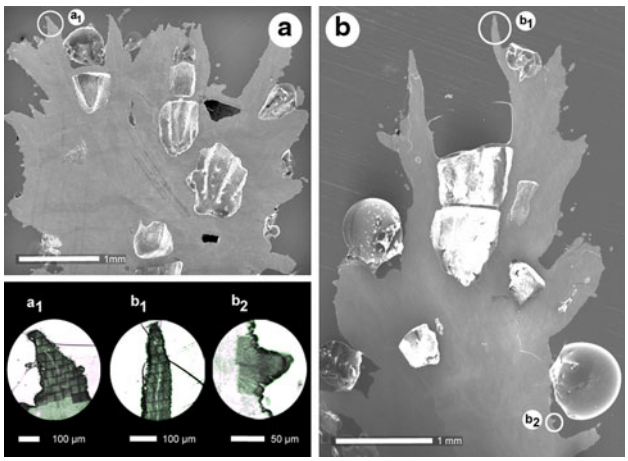

Fig. 3 SEM images of skeletal sections of apical corallites of two different nubbins (**a**, **b**) labeled with ^{86}Sr. Images a_1, b_1 and b_2 (reflected light microscopy) show the square traces of the NanoSIMS sputtering into the surface after analyses. The corresponding mosaics of individual ^{86}Sr/^{44}Ca images obtained with the NanoSIMS from these three regions are shown in Figs. 4 and 5

about 11.6 over the natural ^{86}Sr/^{44}Ca ratio (Fig. 4a), consistent with the TIMS measurements.

Combined NanoSIMS and SEM images of the lightly etched analyzed surfaces (Figs. 4, 5) allow for an interpretation of the skeletal growth dynamics resolved in both time and space at the ultra-structural level. There are two main ultra-structural components in the coral skeleton. Traditionally, these two types of structures have been referred to as "centers of calcification" (COC) and 'fibers', respectively. In the following, we use the nomenclature in which COCs are referred to as Rapid Accretion Deposits (RAD) and fibers are referred to as Thickening Deposits (TD) following Stolarski (2003) (also used in Brahmi et al. 2010; Budd and Stolarski 2011; Janiszewska et al. 2011); c.f. ESM for more detailed discussion.

In the wall at the tip of the corallite (Fig. 4a), the ^{86}Sr-labeled RAD zones are thicker and distances between them are much larger than in the adjacent TD structures. In the spine (Fig. 5e), the ^{86}Sr-labeling is discontinuous and the growth rate significantly lowers, demonstrating that the skeletal growth is a highly heterogeneous process, both temporally and spatially. If skeletal growth had been substantially disturbed, or stopped, during the labeling process, this would clearly leave a mark in the ultra-structure, which we have not observed in the many sections of these corals that we have studied.

Average extension rate determinations at the ultra-structural length scale

The techniques described here allow for a comparison of average extension rates between the ultra-structural components during and between labeling events, in different parts of the skeleton (Fig. 6). Caution is required in the interpretation of such images (Figs. 4, 5). Depending on the orientation of the cut surface relative to the orientation of the labeled ultra-structures (perpendicular vs. tangential, revealed by SEM), different interpretations of the growth dynamics might be obtained. For example, each of the three ^{86}Sr-labeling events exhibited in Fig. 4 lasted precisely 48 h and were separated by 5 days. The first ^{86}Sr-label, which is deepest inside the skeleton, is relatively continuous but does not include RAD structures. This ^{86}Sr-label is only recorded in TD structures (c.f. Fig. 4a–c) that, judging from the SEM image and the width of the ^{86}Sr-labeled layer, were cut perpendicularly by the sectioning of the corallite. The second ^{86}Sr-label includes both TD and RAD regions, the latter being distinctly visible in the corresponding SEM image (Fig. 4c–e). Finally, the last ^{86}Sr-label in Fig. 4a is also exclusively captured in TD structures, with some loss of labeled skeleton at the upper left and top surface of the structure during sample preparation.

The ^{86}Sr-labeled RAD structure is significantly wider than the labeled TD layers, indicating substantially faster growth, consistent with the term 'Rapid Accretion Deposits' to describe these structures (Stolarski 2003). A similar relationship between the extension rate of TD and RAD structures is evident in Fig. 5, showing that the inference about faster average extension of RAD relative to TD is robust and not an artifact created by the orientation of the section.

Average extension rates of RAD and TD were quantified by measuring the width of the ^{86}Sr-labels and the unlabeled layers in-between, in the directions indicated by arrows in Figs. 4 and 5. For the TD structure, a total of 240 measurements in Figs. 4a and 5a were combined to yield an average of 4.1 (±2.3) (SD) µm/day. For the RAD, six measurements yielded an average of 18.3 ± 3.6 (SD) µm/day, a factor of ~4.5 times that in TD. Despite the variations, especially in the TD structures, the inferred difference in average extension rate between RAD and TD in this part of the skeleton is significant.

Importantly, average TD extension rates inferred from the skeleton formed between the labeling events, that is, while the corals resided in the large aquarium with normal seawater, are identical to the average TD extension rates obtained in the labeled parts of the skeleton (Fig. 6). This provides an indication that changes to the physicochemical conditions (e.g., alkalinity and pH) during labeling did not prevent the corals from producing skeleton. It should also be noted that the average extension rates obtained are valid for the apical part of the corallite and should thus be considered maximum values for the coral during the experiment.

In the spine below the tip of the corallite, the average extension rates were lower and more variable (Fig. 5e–g).

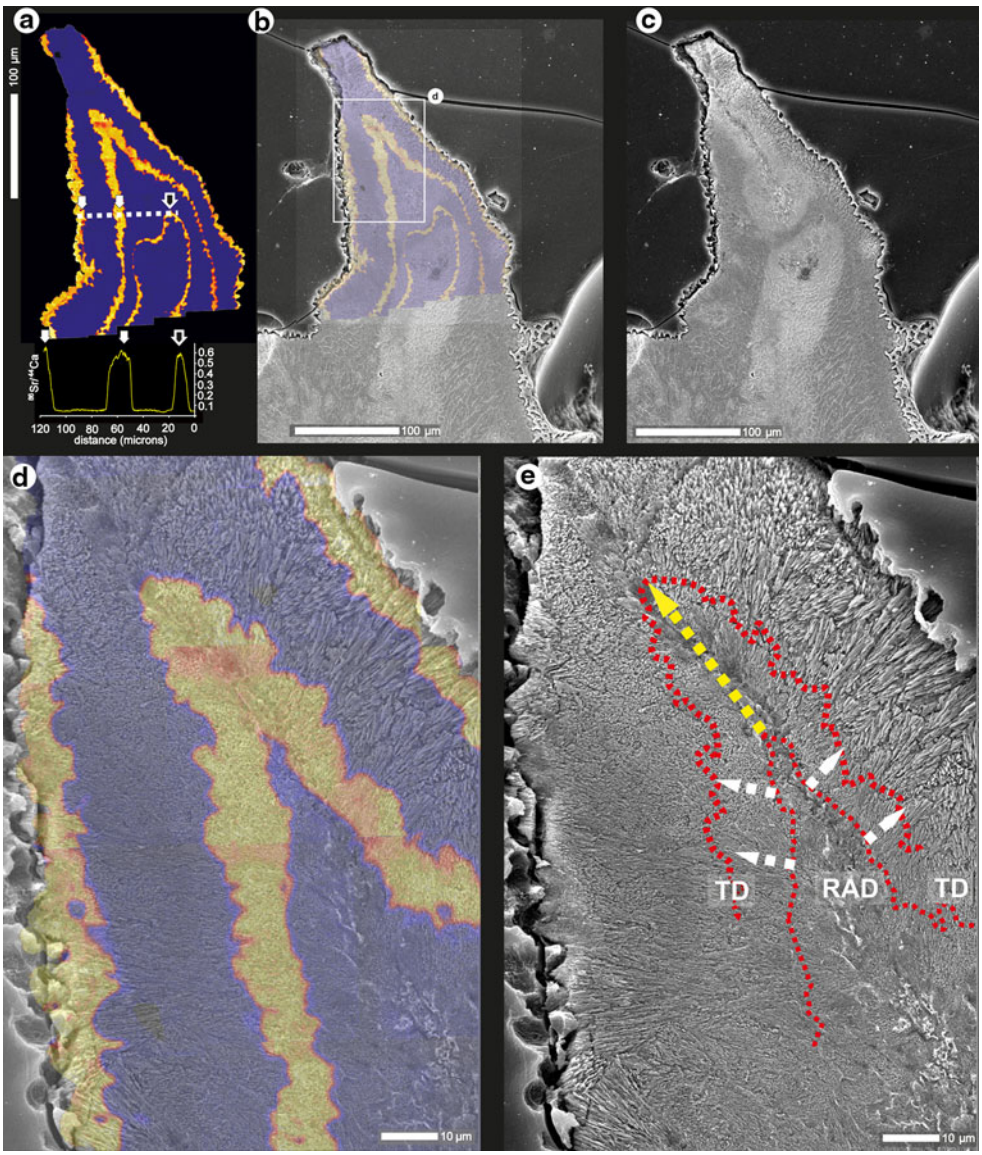

Fig. 4 Mosaic of NanoSIMS $^{86}Sr/^{44}Ca$ maps of the skeletal region indicated in Figs. 3a and a_1. Skeleton formed during growth in seawater enriched in ^{86}Sr has enhanced $^{86}Sr/^{44}Ca$ ratios by a factor of ~11.6 (line-scan *inset* in **a**) and appear *orange-yellow* in color. *Blue* regions represent skeleton with normal $^{86}Sr/^{44}Ca$ ratio. All three ^{86}Sr-labeling events are clearly visible (in the very apical part of the skeleton in Fig. 4a the outermost layer was broken during sample preparation). Subsequent to NanoSIMS analyses, the surface of the imaged region was lightly etched and SEM images (**c**, **e**) were combined with the NanoSIMS mosaics (**b**, **d**). The location of ^{86}Sr-enriched skeleton is outlined in *red* (**e**), with identification of areas of Rapid Accretion Deposits (RAD, *yellow dashed arrow*) and Thickening Deposits (TD, *white dashed arrows*)

Interestingly, at these relatively low growth rates, the ^{86}Sr-label became discontinuous and concentrated in 'hotspots'. This is qualitatively similar to the observations made by Houlbrèque et al. (2009) albeit on a different coral (*Porites porites*).

Discussion

By dissolving 15 mg of $^{86}SrCO_3$ in 1 liter of seawater, the total Sr-concentration increases by only a factor of ~2 (to ~16 ppm), while the $^{86}Sr/^{88}Sr$ ratio increases by a factor of ~11.6. Thus, for a minor change in seawater chemistry, a substantial change in Sr isotopic composition is achieved, resulting in formation of coral skeleton with corresponding ^{86}Sr-enrichments that can be imaged at high spatial resolution (≤500 nm) using a NanoSIMS.

Cellular biomarkers are used to indicate variations in the physiological condition of corals in response to environmental change such as chemical pollution. To our knowledge, this study is the first to use complementary ecotoxicological assays to assess potential physiological

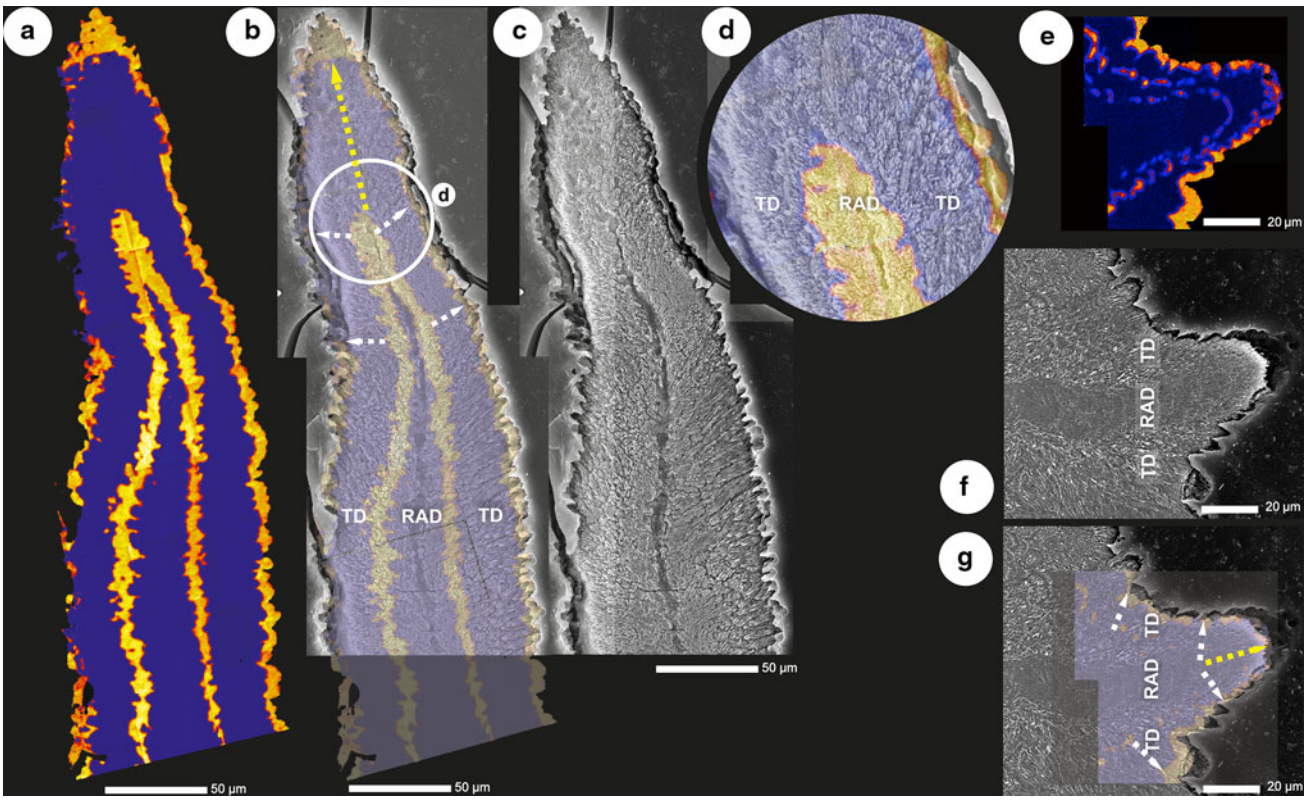

Fig. 5 Mosaic of NanoSIMS $^{86}Sr/^{44}Ca$ maps of the skeletal region indicated in Figs. 3b, b_1 and b_2. Skeleton formed at the tip of the corallite (**a**) during growth in ^{86}Sr-enriched seawater appears *orange-yellow* in color. *Blue* regions represent skeleton with normal $^{86}Sr/^{44}Ca$ ratio. In **a** only the last two ^{86}Sr-labeling events were included in the NanoSIMS map. Subsequent to NanoSIMS analyses, the surfaces of the imaged region were lightly etched and SEM images (**c**, **f**) were combined with the NanoSIMS mosaics in **b**, **d** and **g** along with identification of Rapid Accretion Deposits (RAD, *yellow dashed arrow*) and Thickening Deposits (TD, *white dashed arrows*). **e**–**g** show a spine protruding from the coenosteum (i.e., between corallites) of a nubbin, 4 mm below the growing tip (c.f. Fig. 3b, b_2)

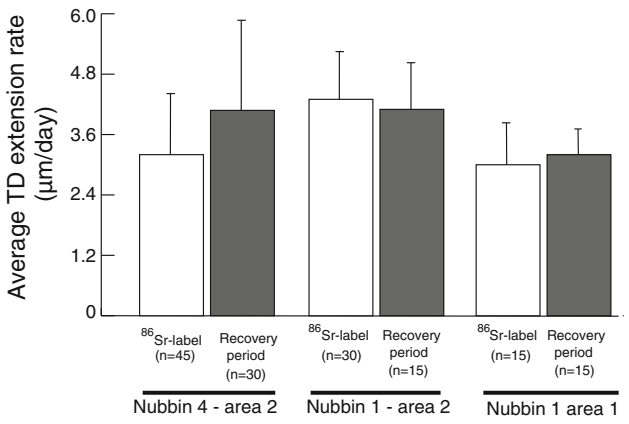

Fig. 6 Average extension rates (µm/day) measured in the Thickening Deposits (TD) of the skeleton formed during the ^{86}Sr-labeling events and during the recovery periods. Data are presented for three different analyzed areas from two nubbins as the mean (±SD). There is no statistical difference between average TD extension rates during periods of ^{86}Sr-labeling and during periods in normal seawater

stress at the cellular level for scleractinian corals during skeletal labeling. Two non-specific stress cellular biomarkers were used (GST activity and porphyrin concentration), and a marker involved in the carbonate biomineralization process (carbonic anhydrase activity).

An increase in glutathione-S-transferase (GST) activity is an indication that the organism is under oxidative stress from what it perceives as a toxic environment (Sies 1999). Shifts in porphyrin concentration reflect changes in cellular metabolism that can be related to stress (Thunell 2000). Carbonic anhydrase (CA) enzymes are ubiquitous metalloenzymes involved in carbonate biomineralization in invertebrates (Wilbur and Jodrey 1956; Gaume et al. 2011). These enzymes catalyze the reversible hydration of carbon dioxide into bicarbonate ions and protons: $CO_2 + H_2O \Leftrightarrow HCO_3^- + H^+$. The involvement of CA in coral biomineralization was first demonstrated by Goreau (1959) for *Porites divaricata*, *Cladocora arbuscula* and *Oculina diffusa* and then confirmed by subsequent studies (Isa et al. 1980; Furla et al. 2000; Al-Horani et al. 2003). A α-CA enzyme was sequenced and its expression localized to the calicoblastic epithelium of the zooxanthellate coral *Stylophora pistillata* (Moya et al. 2008), which is in direct contact with the skeleton and involved in the carbonate formation processes. A decrease in CA activity could signal a perturbation of calcification activity.

All three assays are used in coral ecotoxicology to detect a potential cellular stress in response to a chemical toxicant. Increased GST activity and shifts in porphyrin metabolism were demonstrated in *Porites lobata* (Downs et al. 2006) and in *P. damicornis* (Rougée et al. 2006) exposed to hydrocarbon petroleum (fuel oil). Decreased carbonic anhydrase activity was reported in *Montastraea cavernosa* (Gilbert and Guzman 2001), *Acropora cervicornis* and *Montastraea faveolata* (Bielmyer et al. 2012) in response to seawater contamination.

Our results showed no significant changes in GST activities and in porphyrin concentrations between control nubbins and ^{86}Sr-labeled nubbins and nubbins exposed to enhanced Sr-doses (Fig. 1, ESM Table 1). This biomarker stability indicates that the coral was not experiencing cellular stress by the addition of Sr to the seawater at the levels applied in this study. Moreover, no evidence for potential perturbations to the carbonic anhydrase-related physiological processes involved in calcification was detected during the ^{86}Sr-labeling experiment (Fig. 2, ESM Table 1).

Several studies on zooxanthellate corals have demonstrated a correlation between environmental stress and changes in photosynthesis yield of zooxanthellae symbionts in response to decreasing seawater salinity (Downs et al. 2009) and to contamination with cyanide (Jones and Hoegh-Guldberg 1999) or copper (Bielmyer et al. 2012). Our results showed no significant differences between control and ^{86}Sr-labeled nubbins, indicating that exposure to enhanced Sr-concentrations (and enhanced ^{86}Sr) does not affect the photophysiology of the coral symbionts.

In summary, results of the complementary ecotoxicity assays indicate that fundamental biological processes in the corals were not affected by the addition of Sr (or ^{86}Sr) to the seawater during labeling.

Our combined NanoSIMS and SEM observations of the ^{86}Sr-labeled skeletal microstructure of *P. damicornis* indicate that there is a significant difference in average extension rates of RAD and TD. The average RAD extension rate is 18.3 ± 3.6 (SD) μm/day, a factor of ~4.5 higher than the average extension rate of 4.1 ± 2.3 (SD) μm/day inferred for TD, suggesting different cellular level activities associated with the formation of each ultrastructural component. Shorter (i.e., subdaily) ^{86}Sr-labeling periods would allow a more detailed determination of the spatial and temporal heterogeneity of skeletal formation, which was detected with SEM in *Acropora cervicornis* and *P. damicornis* (Gladfelter 1983; Le Tissier 1988).

The three biomineralization fronts visualized by growth in ^{86}Sr-enhanced seawater are each equivalent to 48 h of growth and are separated by 5 days of growth in unlabeled natural seawater. These growth fronts appear continuous in the fastest-growing apical part of corallum wall, but discontinuous with a hotspot distribution in the spine. A similar 'hotspot' growth front was observed by Houlbrèque et al. (2009) in a slow-growing *Porites porites* coral, after ^{86}Sr labeling for 72 h. In the situation where the exposure to the ^{86}Sr-enriched seawater is short compared to the local growth rate, the result is apparently a discontinuous or hotspot-type of ^{86}Sr labeling in the skeleton. This suggests that the biomineralization front is a highly dynamic interface, where skeletal formation takes place on lateral length scales of about 5 μm along the interface. This typical 5-μm length scale hints that the growth process might be strongly linked to cellular activity in the calicoblastic cell layer (Clode and Marshall 2002; Tambutté et al. 2007b) and/or spatial organization and composition of the skeletal organic matrix (Johnston 1980).

An important general objective in our efforts to develop this method is to find the balance between experimental cost and experimental conditions that allows the organism to biomineralize under essentially unperturbed conditions. The experiments are relatively costly because of the price of purified stable isotopes and the cost of NanoSIMS analyses. It is therefore of interest to identify the minimum isotopic labeling dose and the minimum experimental volume of seawater, which allows the label to be incorporated into the skeleton at levels high enough to be easily imaged by the NanoSIMS, without imposing severe perturbations of the biomineralization processes.

In the experiments presented here, it is obvious that a seawater ^{86}Sr-enhancement by a factor of about 10 is more than enough to make the label in the skeleton easily observable with the NanoSIMS. It would be possible to label with substantially lower ^{86}Sr-enhancements.

Another important issue is the volume during labeling. A balance has to be struck between a small volume that minimizes the costs of the experiment (with ecotoxicology replicates) but is large enough that the physicochemical conditions, such as alkalinity and pH, do not change too much during the labeling event. In this study, a relatively small volume of 250 ml ^{86}Sr-labeled seawater was used. While there is no doubt that alkalinity drops during a 48-h labeling period due to the calcification process, our observations do not indicate that these changes had a strong negative effect on the biomineralization processes. Importantly, the average skeletal extension rates in the TD are statistically indistinguishable between the 48-h labeling periods in the beakers and the 5-day recovery periods in unlabeled, flow-through seawater in an outdoor water table (Fig. 6). Additionally, levels of GST activity and porphyrin concentration (ESM Table 1) fall within the range of background levels measured in *P. damicornis* nubbins maintained in open seawater systems (data not shown). Furthermore, 'test-runs' with similar nubbins of the same species in the exact same experimental conditions indicated

that the pH of the solution dropped by a maximum of 0.2 units, which is within the range of natural daily fluctuations. So, in the experiments presented here, although the 250-ml volume is likely close to the lower limit for a 48-h labeling experiment, the average skeletal extension rates were not affected and no growth stops were observed in the resulting skeleton.

Nevertheless, in future experiments, it is recommended larger volumes of seawater and/or shorter labeling timescales be used in order to minimize potential stress can be minimized. With this in mind, the method developed here is easily expandable to a wide range of marine organisms, using a variety of stable isotope systems depending on the natural chemical composition of the biocarbonates, and can be used to access the growth dynamics under different environmental conditions (pollution, acidification etc.) at high temporal and spatial resolution. Non-marine organisms that form skeletons, teeth, bones etc. can also be studied by these techniques, provided that the uptake of the isotopic label can be facilitated via the substrate on which the organism lives or through its nutrition.

Acknowledgments Collier, B. Gaume, S. Shafir, C. Kopp, J. Martinez and A. Thomen are thanked for fruitful discussions. We gratefully acknowledge support from the Monahan Foundation and the Franco-American commission. This work was supported in part by the European Research Council Advanced Grant 246749 (BIOCARB), the MNHN program ATM "Biomineralizations", grants from the CNRS ("InterVie" and "PIR Interface") and a grant from the Polish Ministry of Science and higher education (project N307-015733). The manuscript has benefited substantially from constructive reviews by Dr. Nicky Allison, Dr. Alex Gagnon and an anonymous reviewer.

References

Adkins JF, Boyle EA, Curry WB, Lutringer L (2003) Stable isotopes in deep-sea corals and a new mechanism for "vital effects". Geochim Cosmochim Acta 67:1129–1143

Al-Horani FA, Al-Moghrabi SM, de Beer D (2003) The mechanism of calcification and its relation to photosynthesis and respiration in the scleractinian coral *Galaxea fascicularis*. Mar Biol 142:419–426

Allison N, Finch A, EIME (2010) δ^{11}B, Sr, Mg and B in a modern *Porites* coral: The relationship between calcification site pH and skeleton chemistry. Geochim Cosmochim Acta 74:1790–1800

Allison N, Cohen I, Finch AA, Erez J, EMIF (2011) Controls on Sr/Ca and Mg/Ca in scleractinian corals: the effects of Ca-ATPase and transcellular Ca channels on skeletal chemistry. Geochim Cosmochim Acta 75:6350–6360

Barnes DJ (1972) The structure and formation of growth-ridges in scleractinian coral skeletons. Proc R Soc Lond B 182:331–350

Bernhard JM, Blanks JK, Hintz CJ, Chandler GT (2004) Use of the fluorescent calcite marker calcein to label foraminiferal tests. J Foraminifer Res 34:96–101

Bielmyer GK, Grosell M, Bhagooli R, Baker AC, Langdon C, Gillette P, Capo TR (2012) Differential effects of copper on three species of scleractinian corals and their algal symbionts (*Symbiodinium spp.*). Aquat Toxicol 97:125–133

Blamart D, Rollion-Bard C, Meibom A, Cuif J-P, Juillet-Leclerc A, Dauphin Y (2007) Correlation of boron isotopic composition with ultrastructure in the deep-sea coral *Lophelia pertusa*: Implications for biomineralization and paleo-pH. Geochem Geophys Geosyst 8 Q12001 doi:10.1029/2007GC001686

Brahmi C, Meibom A, Smith DC, Stolarski J, Auzoux-Bordenave S, Nouet J, Doumenc D, Djediat C, Domart-Coulon I (2010) Skeleton growth, ultrastructure and composition of the azooxanthellate *Balanophyllia regia*. Coral Reefs 29:175–189

Budd AF, Stolarski J (2011) Corallite wall and septal microstructure in scleractinian reef corals: Comparison of molecular clades within the family Faviidae. J Morphol 272:66–88

Bumguardner BW, King TL (1996) Toxicity of oxytetracycline and calcein to juvenile striped bass. Trans Am Fish Soc 125:143–145

Chow TJ, Thompson TG (1955) Flame photometric determination of strontium in seawater. Anal Chem 27:18–21

Clausen CD, Roth AA (1975) Estimation of coral growth rates from laboratory ^{45}Ca incorporation rates. Mar Biol 33:85–91

Clode PL, Marshall AT (2002) Low temperature FESEM of the calcifying interface of a scleractinian coral. Tissue Cell 34: 187–189

de Villiers S (1999) Seawater strontium and Sr/Ca variability in the Atlantic and Pacific oceans. Earth Planet Sci Lett 171:623–634

Dissard D, Nehrke G, Reichart GJ, Nouet J, Bijma J (2009) Effect of the fluorescent indicator calcein on Mg and Sr incorporation into foraminiferal calcite. Geochem Geophys Geosyst 10 Q11001 doi:10.1029/2009GC002417

Dodge RE, Wyers SC, Frith HR, Knap AH, Smith SR, Cook CB, Sleeter TD (1984) Coral calcification rates by the buoyant weight technique: Effects of alizarin staining. J Exp Mar Biol Ecol 75:217–232

Downs CA, Richmond RH, Mendiola WC, Rougée L, Ostrander GK (2006) Cellular physiological effects of the MV Kyowa Violet fuel-oil spill on the hard coral *Porites lobata*. Environ Toxicol Chem 25:3171–3180

Downs CA, Kramarsky-Winter E, Woodley CM, Downs A, Winters G, Loya Y, Ostrander GK (2009) Cellular pathology and histopathology of hypo-salinity exposure on the coral *Stylophora pistillata*. Sci Total Environ 407:4838–4851

Epstein S, Buscsbaum R, Lowenstam HA, Urey H (1953) Revised carbonate-water isotopic temperature scale. Geol Soc Am Bull 64:1315–1326

Ferrier-Pagès C, Boisson F, Allemand D, Tambutté E (2002) Kinetics of strontium uptake in the scleractinian coral *Stylophora pistillata*. Mar Ecol Prog Ser 245:93–100

Finch A, Allison N (2002) Strontium in coral aragonite: 1. Characterization of Sr coordination by extended absorption X-ray fine structure. Geochim Cosmochim Acta 67:1189–1194

Furla P, Galgani I, Durand I, Allemand D (2000) Sources and mechanisms of inorganic carbon transport for coral calcification and photosynthesis. J Exp Biol 158:3445–3457

Gaume B, Fouchereau-Peron M, Badou A, Hellouet M-N, Huchette S, Auzoux-Bordenave S (2011) Biomineralization markers during early shell formation in the European abalone *Haliotis tuberculata*. Mar Biol 158:341–352

Gilbert AL, Guzman HM (2001) Bioindication potential of carbonic anhydrase activity in anemones and corals. Mar Pollut Bull 42:742–744

Gladfelter EH (1983) Skeletal development in *Acropora cervicornis*: II Diel patterns of calcium carbonate accretion. Coral Reefs 2:91–100

Gladfelter EH (2007) Skeletal development in *Acropora palmata* (Lamarck 1816): a scanning electron microscope (SEM)

comparison demonstrating similar mechanisms of skeletal extension in axial versus encrusting growth. Coral Reefs 26:883–892

Goreau TF (1959) The physiology of skeleton formation in corals. I. A method for measuring the rate of calcium deposition by corals under different conditions. Biol Bull 116:59–75

Guzman HM, Cortes J (1989) Growth rates of eight species of scleractinian corals in the eastern Pacific (Costa Rica). Bull Mar Sci 44:1186–1194

Habig WH, Pabst MJ, Jakoby WB (1974) Glutathione-S-transferases. The first enzymatic step in mercapturic acid formation. J Biol Chem 249:7130–7139

Hoogenboom MO, Anthony KR, Connolly SR (2006) Energetic cost of photoinhinition in corals. Mar Ecol Prog Ser 313:1–12

Houlbrèque F, Meibom A, Cuif J-P, Stolarski J, Marrocchi Y, Ferrier-Pagès C, Domart-Coulon I, Dunbar RB (2009) Strontium-86 labeling experiments show spatially heterogeneous skeletal formation in the scleractinian coral *Porites porites*. Geophys Res Lett 36 doi:10.1029/2008GL036782

Ip YK, Krishnanevi P (1991) Incorporation of strontium ($^{90}Sr^{2+}$) into the skeleton of the hermatypic coral *Galaxea fascicularis*. J Exp Zool 258:273–276

Isa Y, Ikehara N, Yamazato K (1980) Evidence for the occurrence of Ca^{2+}-dependent adenosine triphosphatase in a hermatypic coral *Acropora hebes* (DANA). Sesoko Mar Sci Lab Tech Rep 7:19–25

Janiszewska K, Stolarski J, Benzerara K, Meibom A, Mazur M, Kitahara M, Cairns S (2011) A unique skeletal microstructure of the deep-sea micrabaciid scleractinian corals. J Morphol 272:191–203

Johnston IS (1980) The ultrastructure of skeletogenesis in hermatypic corals. Int Rev Cytol 67:171–214

Jones RJ, Hoegh-Guldberg O (1999) Effects of cyanide on coral photosynthesis: Implication for identifying the cause of coral bleaching and for assessing the environmental effects of cyanide fishing. Mar Ecol Prog Ser 177:83–91

Krief S, Hendy EJ, Finea M, Yamd R, Meibom A, Fosterc GL, Shemesh A (2010) Physiological and isotopic responses of scleractinian corals to ocean acidification. Geochim Cosmochim Acta 74:4988–5001

Le Tissier MD'AA (1988) The growth and formation of branch tips of *Pocillopora damicornis*. J Exp Mar Biol Ecol 124:115–131

Lechene C, Hillion F, McMahon G, Benson D, Kleinfeld AM, Kampf P, Distel D, Luyten Y, Bonventre J, Hentschel D, Park KM, Ito S, Schwartz M, Benichou G, Slodzian G (2006) High-resolution quantitative imaging of mammalian and bacterial cells using stable isotope mass spectrometry. J Biol 5 doi:10.1186/jbiol42

Marshall AT, Clode PL (2002) Effect on increased calcium concentration in seawater on calcification and photosynthesis in the scleractinian coral *Galaxea fascicularis*. J Exp Biol 205: 2107–2113

Marshall AT, Wright A (1998) Coral calcification: autoradiography of a scleractinian coral *Galaxea fascicularis* after incubation in ^{45}Ca and ^{14}C. Coral Reefs 17:37–47

Meibom A, Cuif J-P, Mostefaoui S, Dauphin Y, Houlbrèque F, Meibom K, Dunbar R (2008) Compositional variations at ultra-structure length scales in coral skeleton. Geochim Cosmochim Acta 72:1555–1569

Moya A, Tambutté S, Bertucci A, Tambutté E, Lotto S, Vullo D, Supuran C, Allemand D, Zoccola D (2008) Carbonic anhydrase in the scleractinian coral *Stylophora pistillata*: characterization, localization and role in biomineralization. J Biol Chem 282:25475–25484

Nothdurft LD, Webb G (2007) Microstructure of common reef-building coral genera *Acropora*, *Pocillopora*, *Goniastrea* and *Porites*: Constraints on spatial resolution in geochemical sampling. Facies 53:1–26

Rollion-Bard C, Blamart D, Cuif J-P, Juillet-Leclerc A (2003) Microanalysis of C and O isotopes of azooxanthallate and zooxanthellate corals by ion microprobe. Coral Reefs 22:405–415

Rougée L, Downs CA, Richmond RH, Ostrander GK (2006) Alteration of normal cellular profiles in the scleractinian coral *Pocillopora damicornis* following laboratory exposure to fuel oil. Environ Toxicol Chem 25:3181–3187

Sies H (1999) Glutathione and its role in cellular functions. Free Radic Biol Med 27:916–921

Sinclair D (2005) Correlated trace element "vital effects" in tropical corals: A new geochemical tool for probing biomineralization. Geochim Cosmochim Acta 69:3265–3284

Smith SV, Buddemeier RW, Redalje RC, Houck JE (1979) Strontium-calcium thermometry in coral skeletons. Science 204:404–407

Stolarski J (2003) Three-dimensional micro- and nanostructural characteristics of the scleractinian coral skeleton: A biocalcification proxy. Acta Palaeontol Pol 48:497–530

Swart PK, Elderfield H, Greaves MJ (2002) A high-resolution calibration of Sr/Ca thermometry using the Caribbean coral *Montastraea annularis*. Geochem Geophys Geosyst 3 8402 doi: 10.1029/2002GC000306

Tambutté E, Allemand D, Mueller E, Jaubert J (1996) A compartmental approach to the mechanism of calcification in hermatypic corals. J Exp Biol 199:1029–1041

Tambutté E, Allemand D, Zoccola D, Meibom A, Lotto S (2007a) Observations of the tissue-skeleton interface in the scleractinian coral *Stylophora pistillata*. Coral Reefs 26:517–529

Tambutté S, Tambutté E, Zoccola D, Caminiti N, Lotto S, Moya A, Allemand D, Adkins JF (2007b) Characterization and role of carbonic anhydrase in the calcification process of the azoxanthellate coral *Tubastrea aurea*. Mar Biol 151:71–83

Thébault J, Chauvaud L, Clavier J, Fichez R, Morize E (2006) Evidence of a 2-day periodicity of striae formation in the tropical scallop *Comptopallium radula* using calcein marking. Mar Biol 149:257–267

Thunell S (2000) Porphyrins, porphyrin metabolism and porphyries. I. Update. Scand J Clin Lab Investig 60:509–540

Vitale AM, Monserrat JM, Castilho P, Rodriguez EM (1999) Inhibitory effects of cadmium on carbonic anhydrase activity and ionic regulation of the estuarine crab *Chasmagnathus granulata* (Decapoda, Grapsidae). Comp Biochem Physiol C 122:121–129

Wilbur K, Jodrey L (1956) Studies on shell formation V. The inhibition of shell formation by carbonic anhydrase inhibitors. Biol Bull 108:359–365

Zachos J, Pagani M, Sloan L, Thomas E, Billups K (2001) Trends, rhythms and aberrations in global climate 65 Ma to present. Science 292:686–693